International Journal of Physical Sciences vol. 7(44), pp. 5821-5833, 23 November, 2012
Available online at http://www.academicjournals.org/ijps
DOI: 10.5897/IJPS12.356
ISSN 1992 - 1950 ©2012 Academic Journals

Review

Tectonic framework of Lunayyir area, northwest Saudi Arabia through aftershock sequence analysis of 19 May, 2009 earthquake and aeromagnetic data

Al-Zahrani, H. A.[1]*, Fnais, M. S.[1], Al-Amri, A. M.[1] and Abdel-Rahman, K. [1,2]

[1]Geology and Geophysics Department, Faculty of Science, King Saud University, Riyadh, Saudi Arabia.
[2]Seismology Department, National Research Institute of Astronomy and Geophysics, Cairo, Egypt.

Accepted 3 July, 2012

Permanent and temporary seismic stations that were deployed at Lunayyir area before and shortly after the occurrence of the 19 May, 2009 earthquake swarm (M_w 5.7) have recorded a number great of events. The main objective is to determine the tectonic framework of the area and prepare more representative tectonic model for the area. Through the detailed analysis of aftershock sequence it is clarified that; 1) the major part of the cumulative seismic moment has been released after the occurrence of the largest aftershock (m_b 4.8) during the first hours after the main shock; 2) except the first day (20 May, 2009), no event with local magnitude above 4.0 was recorded during the observation period; 3) their distribution oriented NE and NW; 4) it is clustered at two depths; from 5 to 10 and 15 to 25 km beneath Lunayyir area; 5) it is characterized by successive periods of maxima and minima; and 6) the number of aftershocks decayed rapidly after the occurrence of the mainshock following the relation of $n(t)=37.28\ t^{-0.6}$ within the first two weeks and changed later for the other two weeks. Fault plane solutions for eighty-four events indicated normal faulting mechanism for the majority of events while strike-slip components accompanied some of the events. Aeromagnetic maps for Lunayyir area confirmed the presence of shallow and deep-seated faults oriented NE and NW. NE (transform fault) trend runs across the Red Sea into a Shield area and could be interpreted as a channel of magma connecting the Red Sea and Lunayyir area. Whereas, NW (Najd system) faults are predominant through the Shield area and intersected with NE fault trend underlying Lunayyir area. Upwelling magmatic intrusions was initiated at the intersected points causing earthquake swarm. Then, Lunayyir area is highly affected by the present-day Red Sea active tectonics.

Key words: Tectonic framework, Lunayyir area, earthquakes, faults.

INTRODUCTION

Harrat Lunayyir is located in the northwestern part of Saudi Arabia between Latitudes 25°.1- 25°.17 N and Longitudes 37°.45 - 37°.75 E, occupying a surface area of about 3575 Km^2 (Figure 1). It is oriented northwest–Southeast (Laurent and Chevrel, 1980; Al-Zahrani, 2010). Morphologically, there are great variations in the altitudes between hills and wadies through the area. In October 2007 Lunayyir area experienced an earthquake swarm (related to the uplifted magmatic dyke intrusions), where the maximum magnitude was 3.2. In 2009 an earthquake swarm reactivated on 19th April and increased gradually till its maximum on 19th of May where the main shock was observed (M_w 5.7). The main shock was followed by a great number of aftershocks with maximum magnitude (M 4.8) reported on 20 May after some hours from the mainshock occurrence. The origin of this earthquake swarm was volcano-tectonic due to the magmatic dyke intrusions into the crust (Al-Amri and Fnais, 2009; Zahran et al., 2009). This earthquake activity was close to some urban communities (e.g. Al Ays town, 40 km Southeast of

*Corresponding author. E. mail: alzahrani.h@hotmail.com.

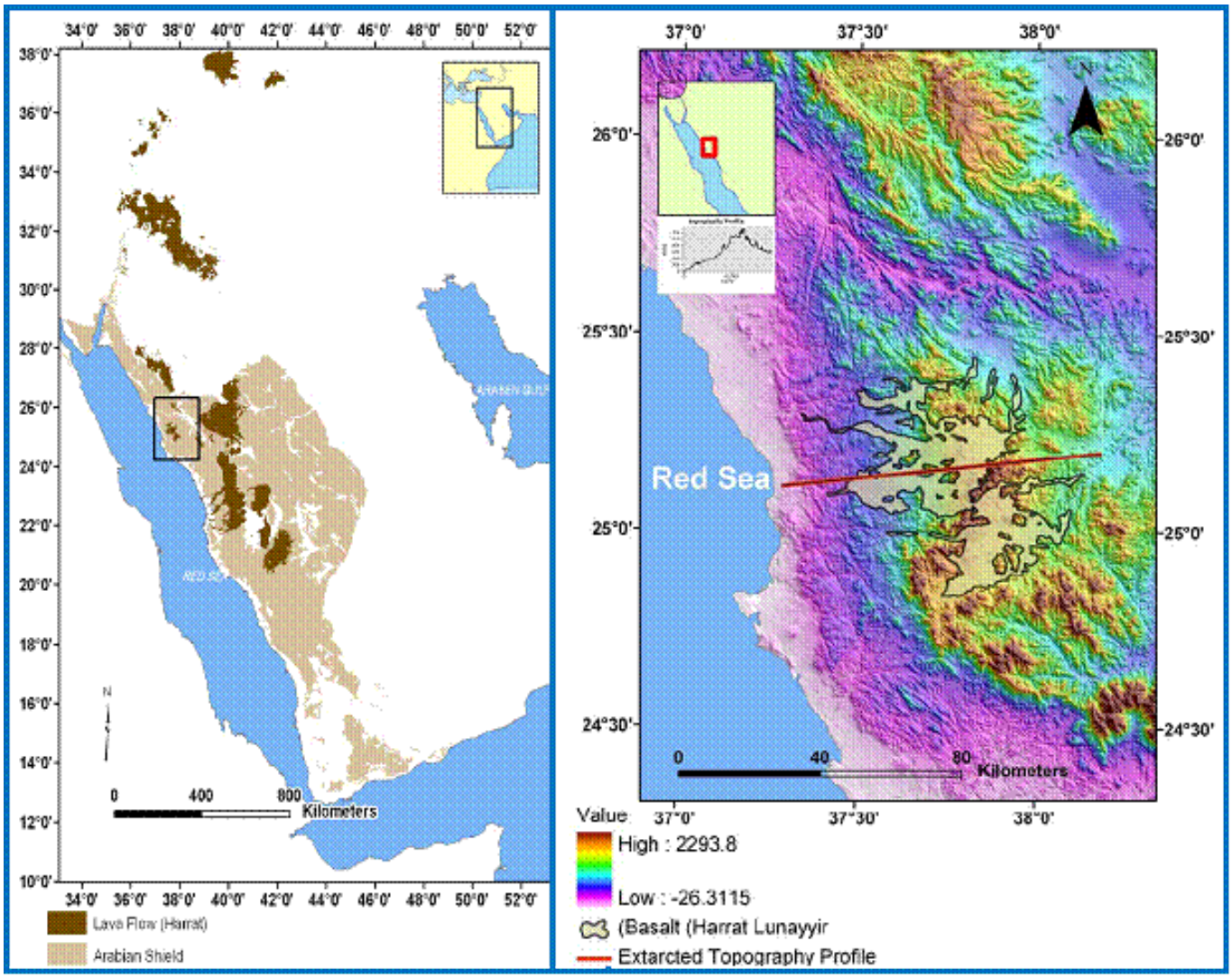

Figure 1. Location and topography of Harrat Lunayyir.

the epicenter). Accordingly, Saudi government evacuated more than 40,000 people (Pallister et al., 2010) from the affected region into Yanbu Al-Bahr (along the Red Sea coast) and Al-Madinah Al-Monawarah.

Depending on the detailed field survey immediately after the mainshock occurrence (Zahran et al., 2009; Fnais, 2010), the epicentral area shows an east-west extension of over 1 m width and uplifted to over 40 cm bounded by a single fault to the southwest showing up to 1 m of faulting and by multiple smaller faults and cracks to the northeast (Jónsson et al., 2010). While the total length of surface rupture was extended up to 8 km and 90 cm of offset with the main shock. Accordingly, the total seismic moment has been calculated through this study as $M_0 = 8.64 \times 10^{24}$ dyne/cm using the relation of $\Delta\sigma = 2.5 M_0/(S)^{3/2}$ (Fukao and Kikushi, 1987) where S is the rupture area that can be estimated by L×(L/2), where L, is the length of surface rupture. Hence, the estimated average stress drop, Δσ, for the mainshock to be about 18.1 bars. It is known that the stress drop on the fault plane due to the occurrence of an earthquake produces an increase of effective shear stress around the rupture area (Chinnery, 1963).

This transfer in the static stress may explain the generation and location of some of the aftershocks at large distances from the fault.

GEOLOGICAL AND TECTONIC SETTING

Lunayyir area is characterized by the presence of hard rocks and soft sediments ranging in age from Precambrian to Recent (Figure 2). Precambrian rocks represented by; 1) Farri group (of lavas, tuff, clastic

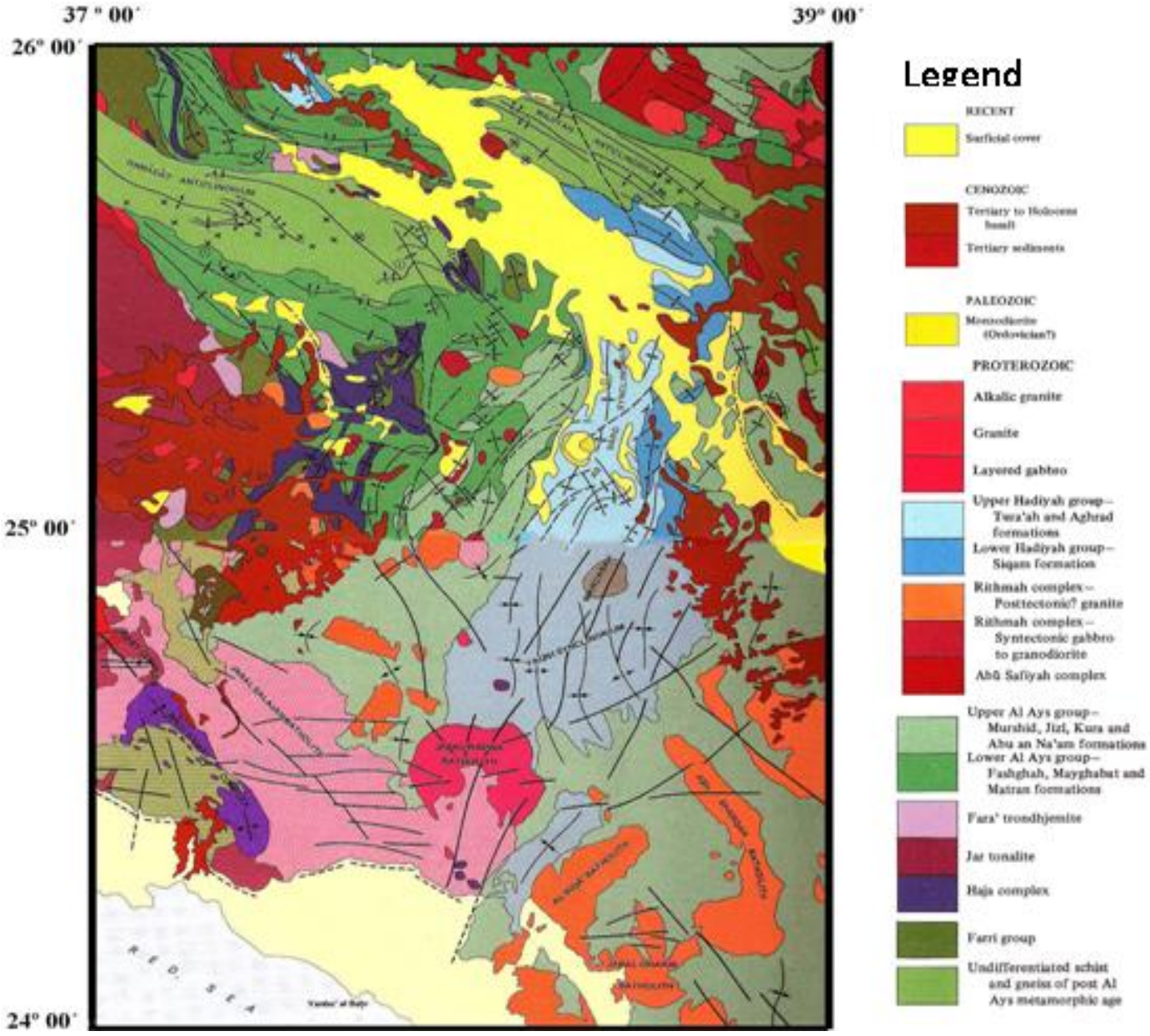

Figure 2. Geological setting around Harrat Lunayyir area.

sediments and limestone's); 2) Al-Ays group (of gneisses and schists that had been subjected to strong folding and faulting); 3) Haja complex (of layered ultramafics); and 4) post tectonic intrusive rocks (of Safiyah Complex, Rithma Complex and Wadi Kamal Complex). While Tertiary sediments composed of marine sediments, coastal deposits, conglomerate and limestones. Furthermore, Tertiary to Holocene basalts composed of alkaline olivine basalt. Whereas Quaternary sediments covering the coastal strip and extends inland along some Wadies (e.g. Wadi Jizl and Wadi Al Hamd) in the northern part of the area.

Tectonically, Harrat Lunayyir was affected by two episodes of tectonic movements synchronized with the Red Sea floor spreading through pre-early Miocene rifting period (Girdler, 1969; Anon, 1972; Rose et al., 1973). Furthermore, it is controlled-to a great extent-by the regional stress regime of the western Arabian plate associated with the Cenozoic development of the Red Sea. Harrat Lunayyir probably faulted during Cenozoic rift time where the uparching period was parallel to the Red Sea coast. During Late Miocene - Pliocene, the alkalic basalt invaded into the Harrat Lunayyir. Consequently, there are different fault trends prevailing the area and

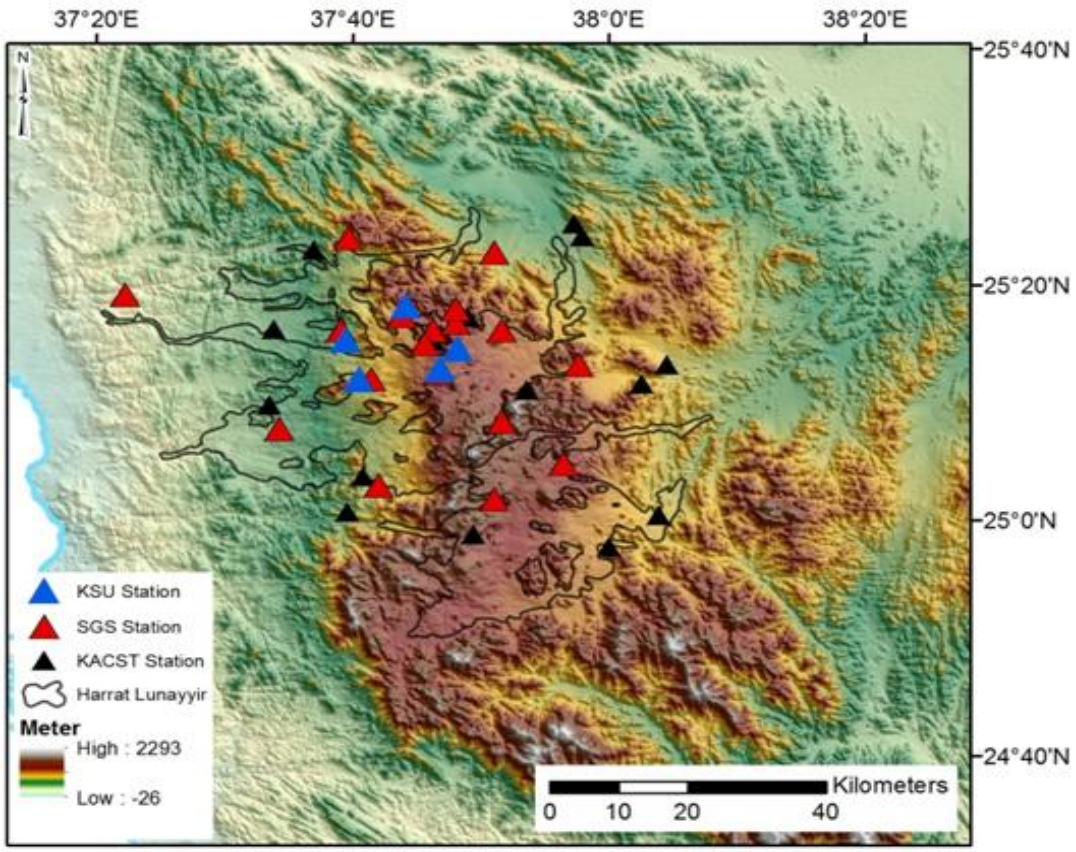

Figure 3. Location map for the deployed stations at the Lunayyir area.

oriented NE- SW, NNW-SSE, and NW-SE.

RECORDING OF AFTERSHOCK SEQUENCE

Saudi geological survey (SGS) deployed a number of permanent broadband seismic stations at Lunayyir area on April 2009 immediately after an outbreak of earthquake activities. Furthermore, shortly after the mainshock occurrence (on 19 May), two cities, King AbdulAziz City of Science and Technology (KACST) and King Saud University (KSU) installed two temporary networks of seismic stations at the affected area of Lunayyir on 20 May for recording and consequent investigation, in details, the behavior of aftershock activities (Figure 3 and Table 1).

KACST seismic network consists of 10 short-period single component (vertical) seismic stations and one Broad band, while KSU network composed of 8 seismic stations of short period with the same configuration of KACST stations. Each of the short period seismic stations includes short period sensor (SS-1 seismometer), Quantira digitizer as seismic data logger (Q_{330}), Biler (20GB hard disk) for storing recorded earthquakes; and 12-volt Battery and Solar panel for continuous charging. While, broadband stations were equipped with Streckeisen STS-2 seismometer. The data was acquired with sampling rate of 300 SPS for the broadband and short period as well. The Hard disk was changed every week and moved into the processing center at King Saud University where, the data were retrieved by a sun workstation and processed using Antelope software (Kinemetrics Inc.). The P and S-waves onset times were picked for the hypocentral parameters computation using the modified version of HYPO71PC software (Lee and Valdes, 1985). Through this study, some of the data was subjected into relocation process using HYPOINVERSE software (Klein, 1987) that calculates also the standard errors of hypocentral parameters. In addition, two of 1-D velocity models (Makris et al., 1978; Al-Amri et al., 2008) have been used through for the reprocessed data in this study. The values of residuals for both crustal models were compared. There are no significant differences between the results of HYPO71 and HYOINVERSE programs, where the epicentral difference was no more than 0.5 km. whereas the depths, which were more sensitive to the velocity model perturbations, differed by about 1 km on average. Consequently, it is believed that the hypocentral locations given by Hypo71 were quite realistic. Accordingly, the

Table 1. The coordinates of temporary seismic stations at Harrat Lunnayyir.

Station code	Latitude (N)	Longitude (E)	Elevation (m)	Type of sensor	Data logger
STN01	25.2554	37.7698	1010	STS-2	Q_{330}
STN02	25.0618	37.6792	559	SS-1	Q_{330}
STN03	25.1851	37.8929	946	SS-1	Q_{330}
STN04	25.264	37.7805	970	SS-1	Q_{330}
STN05	25.1637	37.5574	393	SS-1	Q_{330}
STN06	25.1934	38.0424	600	SS-1	Q_{330}
STN07	25.4015	37.9651	600	SS-1	Q_{330}
STN08	25.3823	37.6161	600	SS-1	Q_{330}
STN09	24.9631	37.9994	600	SS-1	Q_{330}
STN10	25.012	37.6592	600	SS-1	Q_{330}
STN11	25.2877	37.8155	956	SS-1	Q_{330}
STN12	25.2708	37.5637	600	SS-1	Q_{330}
STN13	25.0072	38.065	600	SS-1	Q_{330}
STN14	24.9802	37.8231	600	SS-1	Q_{330}
STN15	25.2204	38.0755	600	SS-1	Q_{330}
STN16	25.4202	37.9542	600	SS-1	Q_{330}
KSU01	25.2134	37.7794	1011	SS-1	Q_{330}
KSU02	25.2423	37.8026	957	SS-1	Q_{330}
KSU03	25.303	37.7355	962	SS-1	Q_{330}
KSU04	25.2555	37.6571	551	SS-1	Q_{330}
KSU05	25.1989	37.6743	551	SS-1	Q_{330}

hypocentral parameters for 1050 of well-located aftershocks during the period of observation (20 May till 20 June) have been analyzed through this study (Figure 4).

Figure 4 shows that these aftershocks are directed northeast at the first and change later towards a northwest position. Figure 5 postulated three episodes of maxima through the period of monitoring; from 29 May to 2 June; from 4 to 6 June; and from 11 to 13 June. These episodes were overlapped by three episodes of minima. It is clearly stated in Figure 6, the extension of these aftershocks into 25 km depth beneath Harat Lunayyir; however the majority took place at 5 to 25 km depth. In general, they are clustered at two layers in depth; the first layer from 5 to 10 km, while the second from 15 to 25 km.

RATE OF DECAY FOR AFTERSHOCKS SEQUENCE

Kisslinger (1997) stated that, the first aftershocks which occurs within the first 24 or 48 h after the main shock defines the relevant rupture surface. Several studies carried out around the world during the past years have indicated that, the occurrence rate of aftershocks, N (t) obeys the modified Omori relation (Gheitanchi, 2003; Benito et al., 2004). The empirical relation for the rate of decay estimation has been suggested by Omori (Utsu, 1961). These relations combine the frequency of aftershocks n(t) per unit time t, following the main shock and represented by:

$$N(t) = K/t^{-c}$$

Where K and c are constants and should be estimated for each region.

402 of well-located aftershocks (M ≥2.0) have been used in this study to estimate the rate of decay for Lunayyir earthquake swarm. The cyclic activation for aftershocks was indicated by their heterogeneities. Hence, first month of aftershock observation could be differentiated into three intervals; the first interval from 20 May till 4 June; the second from 5 to 12 June while the third from 13 to 19 June (Figure 6). Each of these intervals has its own rate of decay that differs from the other two as follows;

$N(t) = 37.28\ t^{-0.60}$, with $R^2 = 0.82$ (for the first two weeks),
$N(t) = 20872\ t^{-3.26}$, with $R^2 = 0.7$ (for the third week), and
$N(t) = 5E{+}08\ t^{-5.33}$, with $R^2 = 0.72$ (for the last week)

Where N (t) being the number of events by day, t is the time in days after the main shock, and R^2 is the correlation coefficient. Figure 7 indicates that, there are three different rates of decay through the first month of observation for the aftershocks of M ≥ 2.0. Another noticeable feature for Lunayyir aftershock sequence is the release of a major part of the cumulative seismic moment during the first hours after the main shock. Excluding the first day (20 May, 2009), no event with local magnitude above 4.0 was recorded during the

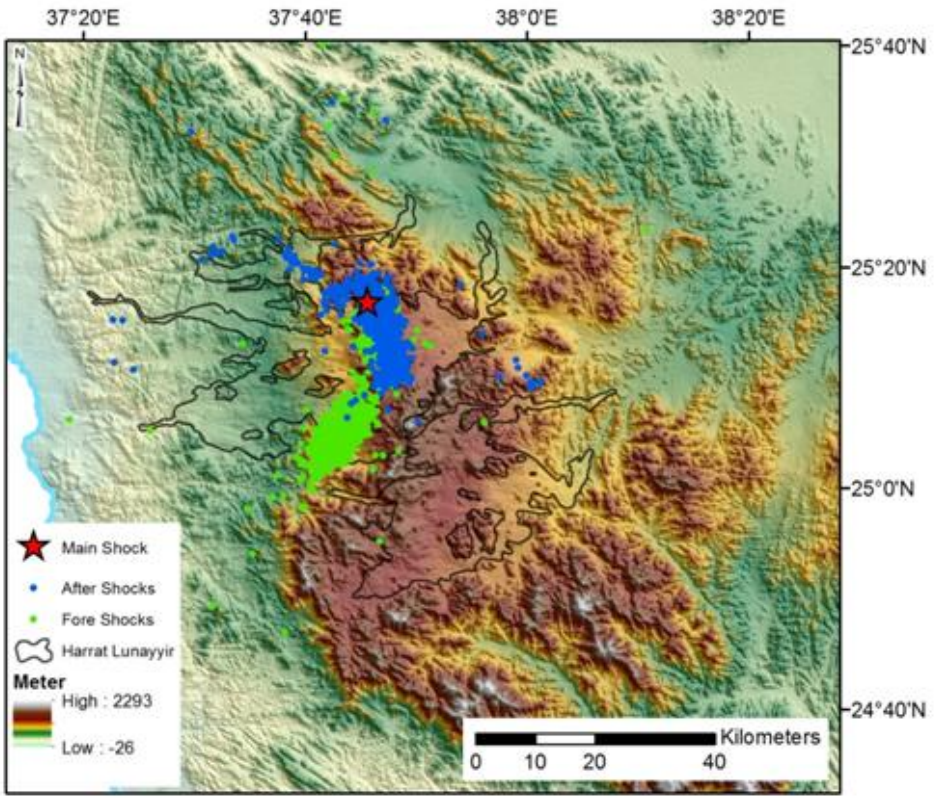

Figure 4. Distribution of the 2009 earthquake swarm at Lunayyir area.

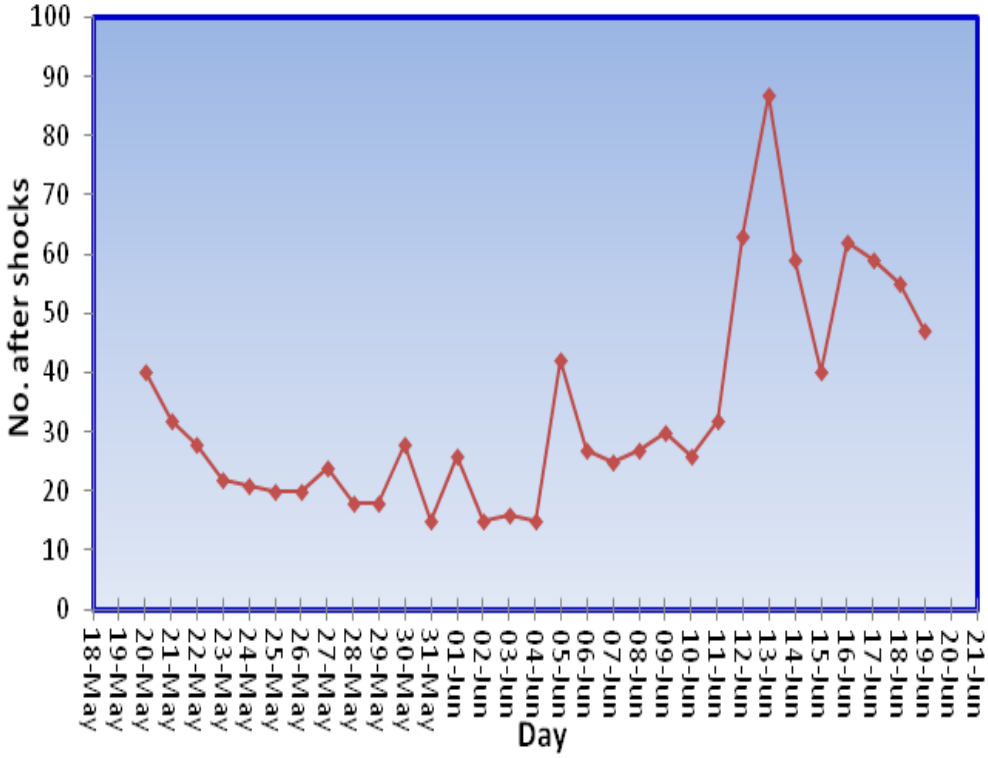

Figure 5. Relationship between number of aftershocks per day.

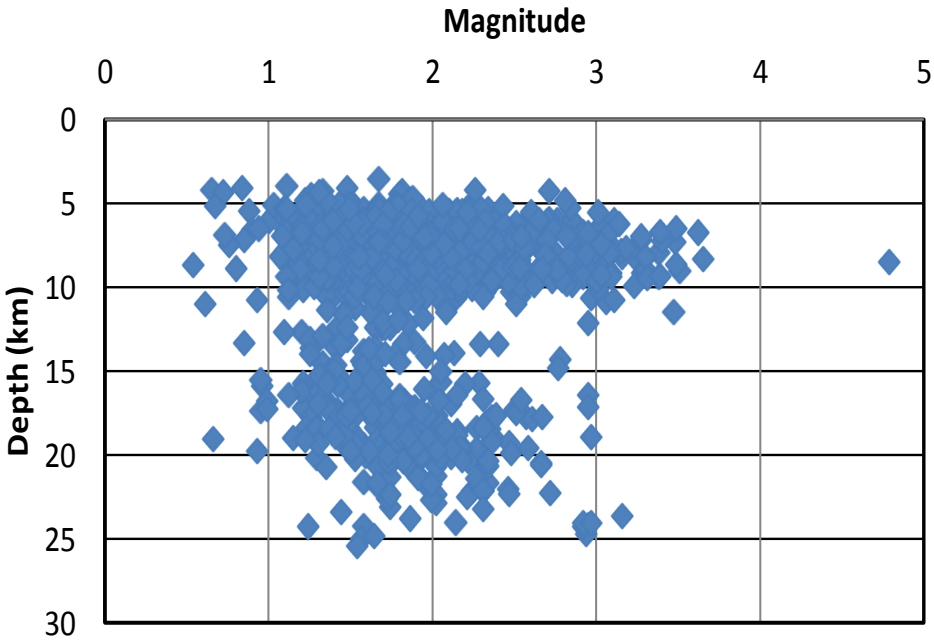

Figure 6. The relationship between magnitude and depth.

period of recording.

FAULT PLANE SOLUTIONS

Depending on the P-wave first motion polarities, fault plane solution of eighty-seven events of 19 May earthquake swarm were calculated using the PMAN program (Suetsugu, 2003), where the information of events before 20 may was gathered from Saudi Geological Survey (SGS) of stations previously installed at Lunayyir area. The input parameters including azimuths and take-off angles were calculated based on a 1-D velocity model (Al-Amri et al., 2008). Figure 8 shows the spatial distribution of the main shock and the selected aftershocks with focal mechanisms shown by equal area projections of the lower focal hemisphere. The parameters of fault plane solutions are listed in Table 2.

There is a wide range of fault plane solutions resulting from the analysis of eighty-four events from the aftershocks where the intersected pattern of fault trends was identified. Not only NE-SW and NW-SE structural trends are prevalent at the Harrat but NNE- SSW or NNW-SSE and N-S also were detected. However, the normal faulting mechanisms represent how common it was accompanied by strike-slip components for some other events. The average trend of extensional axes (T-axes) was extending ENE-WSW while the compressional stress axes (P-axes) oriented NW-SE. These results are in agreement with the mapped ground cracks and fissures (Zahran et al., 2009; Jónsson et al., 2010; Fnais, 2010) immediately after the mainshock occurrence.

AEROMAGNETIC DATA

Total Magnetic Intensity (Figure 9) for Harte Lunayyir and its surroundings provided detailed information for the deep-seated structural elements; faults, shear zones, sutures between Precambrian terranes, and Precambrian and Tertiary dikes, as well as prominent lithologic features such as plutons, dikes. Figure 9 shows the major anomalies, which run parallel to the main axial trough of the Red Sea (NNW). However, other anomalies are offset in a northeasterly (NE) direction that could be due to the magnetic expression of transformed faults. These two directions could intersect under Lunayyir area. The NW trending (Najd system), which dominates the magnetic pattern of the basic dikes, is injected into Najd system. Furthermore, the north-south trending system is encountered and interpreted as being younger than the Najd system where it has been reactivated during the Tertiary period explaining the main trend of harrats (Milton, 1970).

Furthermore, total magnetic intensity map was transferred into RTP map (Reduced To Pole). The regional-residual separation process was done for RTP map to improve the regional, deep seated structures and separate the local and shallow anomalies that could obscure these deep tectonic features. The qualitative interpretation for the regional aeromagnetic map for

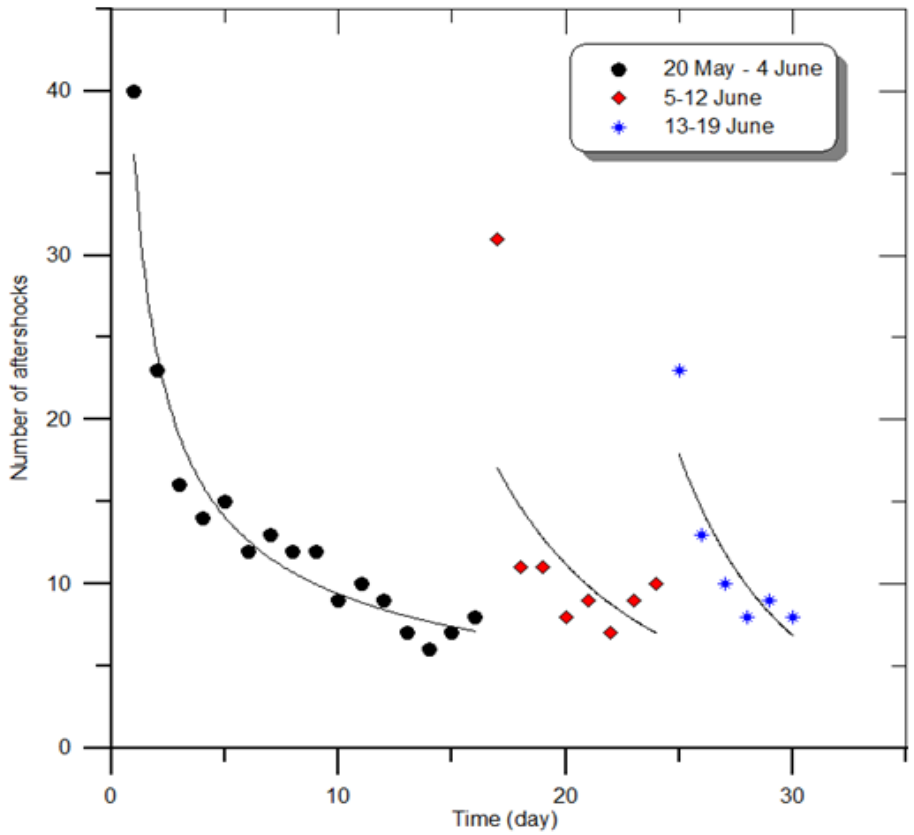

Figure 7. Rate of decay for the aftershock sequence (M ≥ 2).

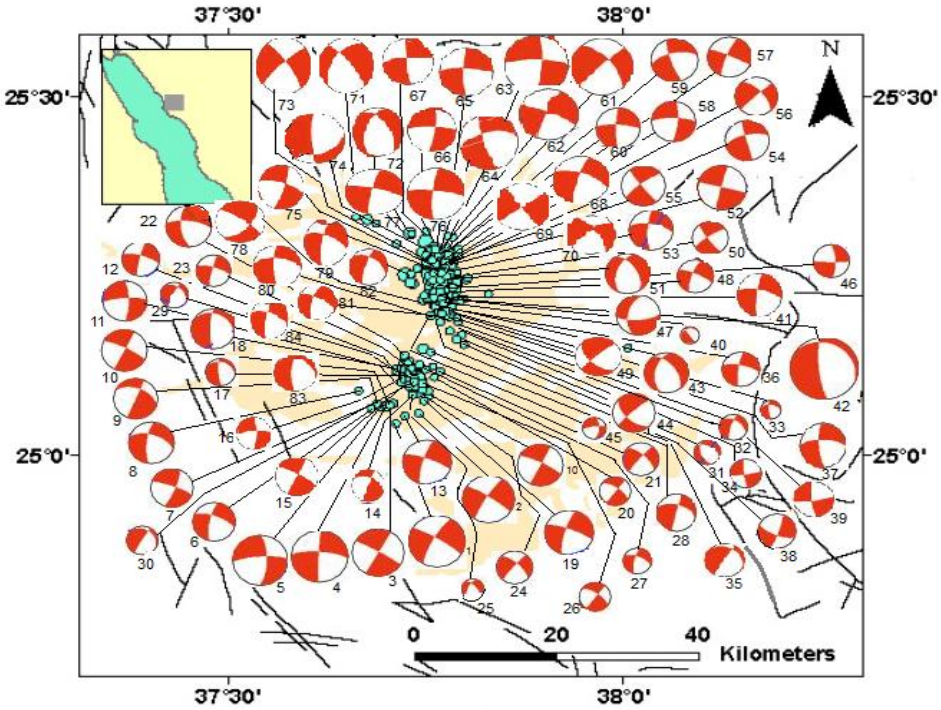

Figure 8. Fault plane solution for some of aftershocks.

Table 2. Fault plane solutions for some selected events of 19 May 2009 earthquake swarm.

No.	Time					M.	Fault plane						Stress plane			
							NP1			NP2			P-axis		T-axis	
	Days	Month	Hour	Minute	Second		St.	Dip	Rake	St.	Dip	Rake	St.	Dip	St.	Dip
1	13	5	18	35	45	3.96	301	81	-169	209	79	-9	165	14	75	1
2	13	5	19	16	13	3.67	303	83	-177	212	87	-7	167	7	258	3
3	13	5	21	41	1	3.63	300	85	-179	210	89	-5	165	4	255	3
4	13	5	23	8	56	4.25	188	81	-15	281	75	-170	144	18	125	4
5	13	5	23	47	18	3.97	274	74	-175	183	85	-16	138	15	230	8
6	14	5	14	1	34	3.85	271	69	-166	176	77	-21	132	24	224	5
7	17	5	19	20	27	4.15	289	71	169	22	80	19	155	6	247	21
8	17	5	19	50	04	4.68	288	74	168	21	79	17	154	4	245	20
9	17	5	20	21	04	4.6	122	86	179	212	89	4	347	2	77	4
10	18	5	7	41	02	4.37	132	84	173	223	83	6	178	1	88	9
11	19	5	0	5	59	3.01	290	66	-162	192	73	-25	149	30	242	5
12	19	5	0	7	46	3.01	290	81	169	22	79	9	-23	1	246	14
13	19	5	0	25	54	3.18	288	57	-159	186	72	-35	143	37	240	10
14	19	5	0	43	56	3.16	292	48	180	23	90	42	149	28	256	28
15	19	5	0	55	50	3.25	297	79	-179	207	89	-11	161	8	252	7
16	19	5	1	4	35	3.13	267	78	164	360	75	12	-46	2	223	19
17	19	5	1	14	54	2.65	286	72	-175	194	85	-18	148	16	241	9
18	19	5	1	51	29	3.48	197	76	-11	290	79	-165	154	18	63	3
19	19	5	2	6	3	1.72	195	88	-10	286	80	-178	150	8	119	6
20	19	5	2	11	33	2.32	293	74	-172	201	83	-16	156	16	248	6
21	19	5	2	17	15	1.67	316	61	-173	223	84	-29	175	25	273	16
22	19	5	2	18	32	2.1	291	25	-151	175	78	-67	111	52	246	29
23	19	5	2	26	41	3.13	300	25	-148	181	77	-68	117	53	253	28
24	19	5	2	38	42	2.55	248	20	158	358	83	72	104	35	249	49
25	19	5	2	50	13	2.39	344	78	59	234	33	157	98	26	220	48
26	19	5	3	2	15	1.98	309	35	-164	206	81	-56	149	44	270	28
27	19	5	3	5	21	3.2	175	61	-24	277	69	-149	139	36	45	5
28	19	5	3	8	4	2.42	286	74	-172	194	82	-16	150	17	241	6
29	19	5	3	10	5	2.52	312	68	-174	220	84	-23	174	20	268	11
30	19	5	3	12	12	1.57	318	63	-141	207	56	-34	175	46	81	4
31	19	5	3	13	35	2.25	306	68	178	37	88	22	170	14	264	17
32	19	5	3	16	11	2.05	103	71	150	203	62	21	154	6	60	34
33	19	5	3	28	36	3.1	193	87	-39	285	51	-176	142	28	-114	24
34	19	5	3	42	13	3.07	287	89	-12	277	78	-179	142	9	-127	7
35	19	5	3	48	20	2.22	211	86	-66	310	24	-170	144	44	-80	37
36	19	5	4	10	49	1.91	156	50	-66	301	46	-116	132	71	-131	2
37	19	5	4	14	48	2.01	303	47	-159	198	75	-45	150	42	257	17
38	19	5	4	47	55	2.92	290	32	-155	179	77	-61	121	49	246	27
39	19	5	5	10	48	2.19	82	84	171	173	81	6	128	2	38	11
40	19	5	5	12	17	1.49	174	73	-47	282	45	-156	126	45	-126	17
41	19	5	5	14	12	2.7	188	79	-20	282	70	-168	144	22	-124	6
42	19	5	5	24	38	3.1	182	82	-26	276	64	-172	136	24	-128	13
43	19	5	5	48	44	2.67	112	70	-169	19	79	-20	334	22	67	6
44	19	5	5	52	54	2.1	285	84	-178	195	88	-6	150	6	240	3
45	19	5	5	56	57	1.28	143	84	-69	249	22	-162	74	47	-145	35
46	19	5	6	1	55	2.86	163	83	-46	259	44	-170	110	36	-140	25
47	19	5	6	38	29	4.81	174	77	-74	303	21	-139	105	56	-109	30
48	19	5	6	41	17	3.14	191	47	126	324	53	58	76	3	173	64

Table 2. Contd.

49	19	5	6	55	43	3.02	134	57	-7	228	84	-147	96	27	356	18
50	19	5	7	3	28	1.68	262	77	147	1	58	15	-45	12	217	32
51	19	5	7	42	33	2.56	90	84	21	358	69	173	-138	10	316	19
52	19	5	7	48	42	3.09	86	71	139	192	52	24	143	12	42	42
53	19	5	7	54	48	2.6	200	73	-15	294	76	-162	158	23	67	2
54	19	5	8	3	11	1.58	179	77	-23	274	67	-166	135	25	-132	7
55	19	5	8	4	52	2.6	144	81	166	236	76	9	-170	4	99	16
56	19	5	8	14	35	3.14	200	49	131	328	55	53	83	4	179	60
57	19	5	10	6	30	3.43	194	87	-9	284	81	-177	149	9	-121	5
58	19	5	10	9	48	3.08	279	66	-167	183	78	-25	139	26	233	8
59	19	5	11	1	1	3.13	256	66	-176	165	86	-24	118	19	213	14
60	19	5	11	9	7	3.12	142	85	172	233	82	5	-172	2	98	9
61	19	5	11	26	24	3.02	319	64	-175	227	85	-26	180	21	276	15
62	19	5	14	53	53	3.12	293	85	-166	202	76	-6	158	13	67	6
63	19	5	15	38	53	3.16	271	75	164	5	75	15	-42	0	228	21
64	19	5	15	50	45	3.34	161	77	-29	258	62	-165	116	30	-148	10
65	19	5	16	10	4	3.14	273	77	-169	181	79	-13	137	17	227	2
66	19	5	16	17	6	3.39	273	74	172	5	82	16	138	6	230	17
67	19	5	16	20	43	3.55	265	75	-175	174	85	-15	129	14	221	7
68	19	5	16	38	28	3.45	290	68	-171	196	81	-23	151	22	245	9
69	19	5	16	54	28	4.9	144	88	178	234	88	2	-171	0	99	3
70	19	5	17	13	26	4.21	325	70	-167	230	78	-21	187	24	279	5
71	19	5	17	34	58	5.39	319	77	43	217	48	163	82	18	187	39
72	19	5	18	20	0	4.29	108	50	130	235	54	53	351	2	85	60
73	19	5	19	21	27	4.01	322	78	-171	230	81	-12	186	14	276	2
74	19	5	19	26	58	4.03	177	81	-127	75	38	-16	52	43	-65	26
75	19	5	19	33	21	3.7	286	73	171	19	81	18	152	6	244	19
76	19	5	19	44	19	3.63	277	79	-173	185	83	-12	141	13	231	3
77	19	5	19	50	43	3.89	284	78	-172	192	82	-13	148	15	238	3
78	19	5	20	35	37	4.25	305	79	149	42	59	13	-3	13	259	29
79	19	5	22	11	54	2.59	293	56	-154	187	69	-37	145	41	243	8
80	19	5	23	18	35	3.18	276	55	-168	179	80	-36	132	32	232	17
81	19	5	23	43	32	3.42	296	67	-156	196	68	-25	155	33	246	1
82	20	5	19	57	16	4.79	116	80	143	214	53	13	170	17	68	33
83	29	5	9	56	15	3.09	311	24	-135	178	73	-73	112	58	255	26
84	30	5	8	31	57	3.49	318	38	-148	202	71	-56	151	52	267	19

Lunayyir area (Figure 10) clarified the main aeromagnetic trends affecting the area; NW (Najd), NE and N-S directions. While the residual map (Figure 11) illustrates that some of the linear anomalies correspond to the intrusive dikes and other circular anomalies reflecting the intrusive bodies.

Conclusions

The aftershocks were concentrated at two depths of 5 to 10 km and 15 to 25 km beneath Lunayyir area. Considering that the depth of the main shock was 9 km, this indicated that the rupture process was initiated at the depth of a main shock and propagated upward and downward in bilateral behavior of directivity. Aftershock sequence was represented by the overlapping cycles of maxima and minima with different numbers and magnitudes. This may reflect the non-homogeneity in stress levels owing to the upward and downward magmatic dyke movements. Most of the accumulated energy was released shortly after the main shock and decreased rapidly with different rates of decay till the end of the observation period. This maybe, explains the presence of small scale ground cracks and fissures intersected with the major ruptures at the epicentral area.

Results of fault plane solutions for eighty-four of

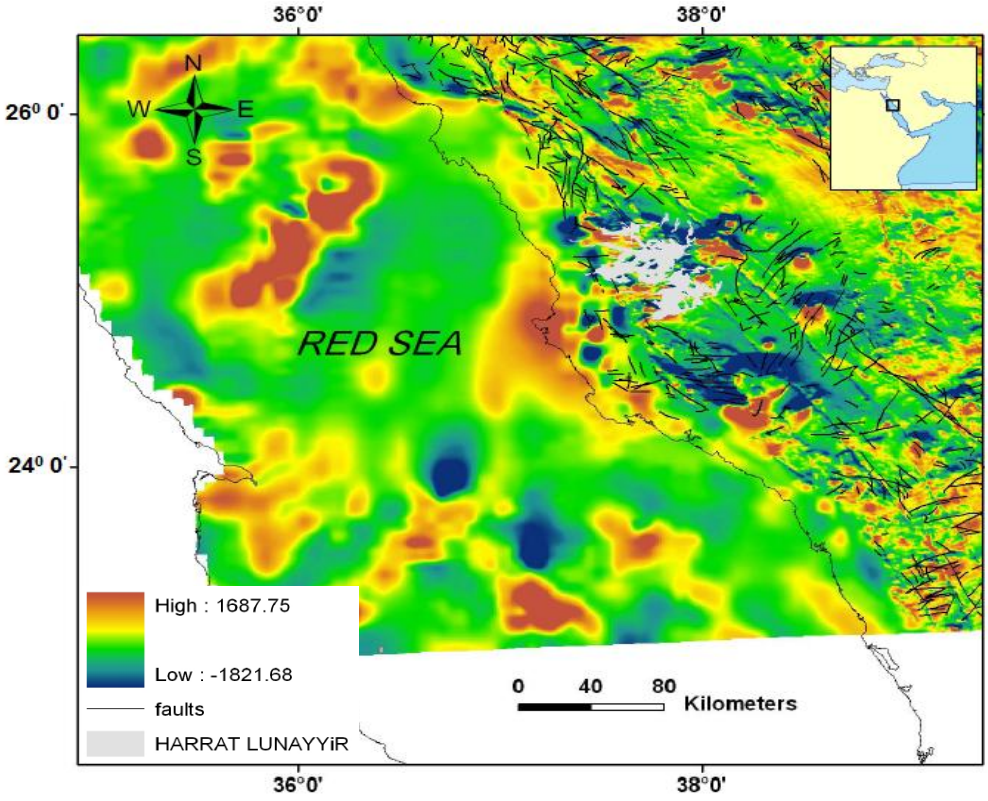

Figure 9. Total aeromagnetic intensity (TMI) map of the study area.

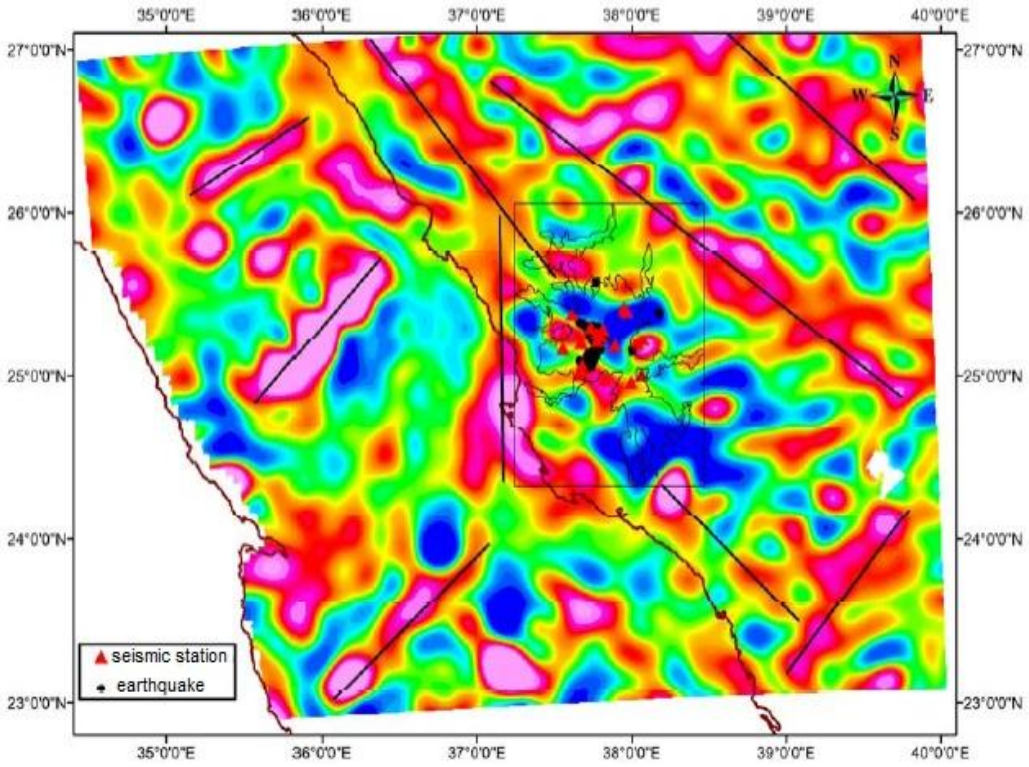

Figure 10. Regional aeromagnetic map of Lunayyir area.

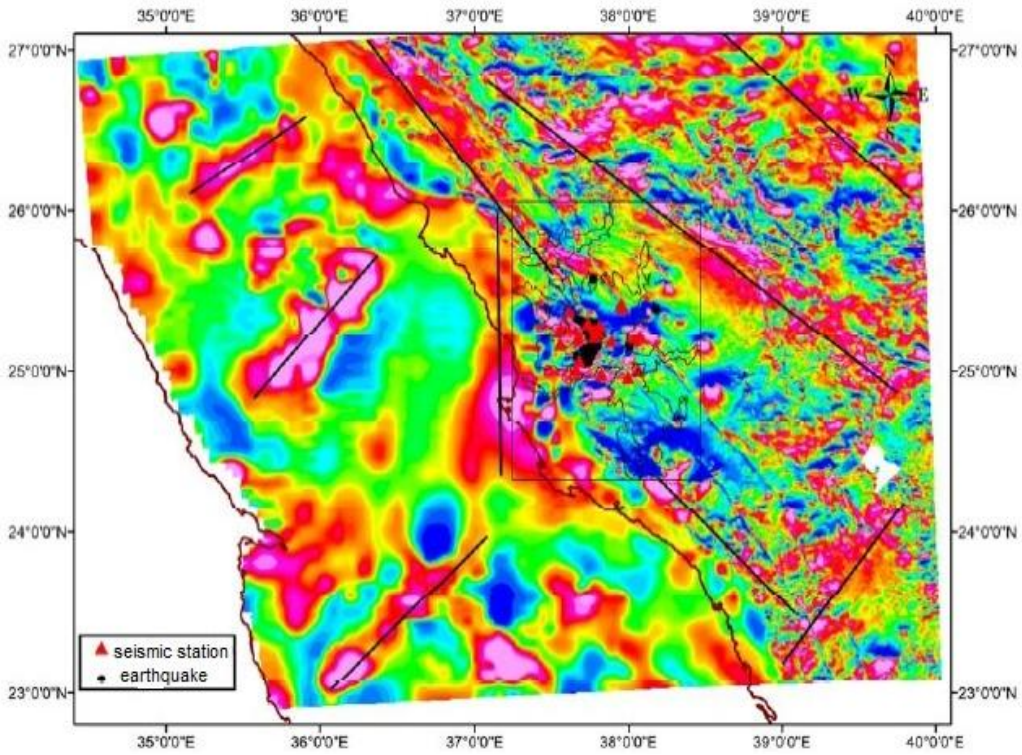

Figure 11. Residual aeromagnetic map of Lunayyir area.

earthquake swarm indicate the complicated tectonic setting of Lunayyir area. There are different fault trends oriented NNE-SSW, NNW-SSE, N-S, NE-SW and NW-SE are identified well with different angles of dip and plunge. Normal faulting is the major mechanism but sometimes was associated with strike-slip components for the other events. NE-SW trend represents the main extensional axis while NW-SE acts the compressional axis. These results clarified the infection of the Lunayyir area with the present-day active tectonics related to the Red Sea floor spreading. Hence, it could be stated that there is great potentialities for the stress accumulations beneath Lunayyir area.

Total magnetic intensity map for Lunayyir area shows that some magnetic anomalies are offset in a northeasterly direction and others are parallel to the axial trough of the Red Sea. NE anomalies could be due to the magnetic expression of transform faults which cause disturbances of the magnetic anomalies. These anomalies are abundant but having a limited extension across the Red Sea extend onto the coastal plain and inland as far as the exposed margin of the shield, where they are associated with the diabase dike swarm.

Regional and residual aeromagnetic RTP maps shows that; 1) The NW trending Najd system which dominates the magnetic pattern of the basic dikes where injected into the Najd system, 2) NNW trending Red Sea system that exists around the Red Sea representing series of Tertiary mafic dikes emplaced during the opening of the Red Sea, 3) N-S trending system, which is younger than Najd system, could be reactivated during the Tertiary, thus explaining the main northerly trend of the most basic Harrats, 4). NE trending system is thus, interpreted as Precambrian system reactivated during the opening of the Red Sea and comprising fundamental basement structures caused by deep sources with extensive roots.

The downward continuation of NE transform faults from the shallow depths (local map) into deeper depths (regional) could be interpreted as the channel of magma connected to the Red Sea and Lunayyir area. These NE faults intersect with the NW (Najd) faults and then intrudes upward into the Earth's surface causing cracking of the crystalline rocks and earthquake swarms. If the generated stresses are great this may lead to the eruption of a volcano at the points of intersection, and this could explain the purification of the ancient volcanoes in the region.

Accordingly, the continuous monitoring for the volcano-tectonic processes and their related environmental hazards at Harrat Lunayyir area are highly recommended.

REFERENCES

Al-Amri A, Rodgers A, Al-khalifah T (2008). Improving the Level of Seismic Hazard Parameter in Saudi Arabia Using Earthquake

Location. DOI 10.1007/s12517-008-0001-5. Arab. J. Geosci. 1:1-15.
Al-Amri AM, Fnais MS (2009). Seismo-volcanic investigation of 2009 earthquake swarms at Harrat Lunayyir (Ash Shaqah), Western Saudi Arabia. Intern. J. Earth Sci. Eng. India (in press).
Al-Zahrani H (2010). An Investigation of Seismo-volcanic Sources of Harrat Lunayyir, NW Al-Madinah Al- Munawwarah. M.Sc. Thesis, Fac. Sci. King Saud Univ. p. 102.
Anon (1972). The Sea that is really an ocean. New Sci. 34:414-445.
Benito B, Cepeda JM, Martinez DJJ (2004). Analysis of the spatial and temporal distribution of the 2001 earthquakes in El Savador, in Rose, W.I., Bommer, J.J., Lopez, D.L., Carr, M.J., and Major, J.J, eds., Natural hazards in El Salvador: Boulder, Colorado, Special paper. Geol. Soc. Am. 375:1-18.
Chinnery MA (1963). The stress changes that accompany strike-slip faulting. Bull. Seismol. Soc. Am. 53:921-932.
Fnais MS (2009). Enhancement of geophysical data using seismic attributes. J. Appl. Geophys. (JAG), EGYPT, 8(1):116-131.
Fnais MS (2010). Coseismic Ruptures caused by 19 May 2009 Earthquake (M_w 5.7), Western Saudi Arabia. Bull. Egypt. Geophys. Soc. EGYPT (in press).
Fukao Y, Kikuchi M (1987). Source retrieval for mantle earthquakes by iterative deconvolution of long-period P-waves. Tectonophysics 144:249-269.
Gheitanch MR (2003). Analysis of the 1990 Fork (Darab), southern Iran, earthquake sequence. J. Earth Space Phys. 29(1):13-19.
Girdler RW (1969). The Red Sea-a geophysical background. In: Degens ET, Ross D. A. (eds): Hot brines and recent heavy metal deposits in the Red Sea. Springer, New York. pp. 59-70.
Jónsson S, Pallister J, McCausland W, El-Hadidy S (2010). Dyke Intrusion and Arrest in Harrat Lunayyir, western Saudi Arabia, in April-July 2009. EGU2010-7704. Geophys. Res. Abstr. P. 12.
Kisslinger C (1997). Aftershocks and fault zone properties. Adv. Geophys. 38:1-35.
Klein RW (1987). Hypocenter location program. HYPOINVERSE, part 1: user guide, open file report. U.S. Geological Survey, Menlo Park, California. P. 113.
Laurent D, Chevrel S (1980). "Prospecting for Pozzolan on Harrat Lunayyir". Ministry of Petroleum and Mineral Resources.
Lee WK, Valdes CM (1985). HYPO71PC: A personal computer version of the HYPO71 earthquake location program. U. S. Geol. Surv. Open File Report pp. 85-749, 43.
Makris J, Allam A, Mokhtar T, Basahel A, Dehghani GA, Bazari M (1978). Crustal structure of northeast region of Saudia Arabia and its transition to the Red Sea. Report, National Research Institute of Astronomy and Geophysics, Helwan, Egypt.
Milton R (1970). Structures geologiques revelees par l'interpretation de leve aeromagnetique du bouclier Arabe. Bureau de Recherches Geologiques et Minieres Bull. 4(2):15-25.
Pallister J, McCausland W, Jónsson S, Lu Z, Zahran HM, El-Hadidy S, Aburukbah A, Stewart I, Lundgern P, White R, Moufti M (2010). Broad accommodation of rift-related extension recorded by dyke intrusion in Saudi Arabia. Nature geoseisnce, Macmillan Publishers Limited. P. 8.
Rose DA, Whitmarsh RB, Ali SA, Boudreaux JE, Coleman RG, Fleisher RL, Girdler R, Manheim F, Matter A, Nigrini C, Stoffers P, Supko PR (1973). Red Sea, drilling. Science 179:377-380.
Suetsugu D (2003). PMAN The program for focal mechanism diagram with p-wave polarity data using the equal-area projection. IISEE Lecture Note, Tsukuba, Japan pp. 44-58.
Utsu T (1961). A statistical study on the occurrence of aftershocks. Geophysics. Mag. 30:521-605.
Zahran HM, McCausland WA, Pallister JS, Lu Z, El-Hadidy S, Aburukba A, Schawali J, Kadi K, Youssef A, Ewert JW, White RA, Lundgren P, Mufti M, Stewart IC (2009). Stalled eruption or dike intrusion at Harrat Lunayyir, Saudi Arabia?. American Geophysical Union, Fall Meeting, abstract V13E-2072.